Metals **2015**, *5*, 439-456; doi:10.3390/met5010439

OPEN ACCESS

metals

ISSN 2075-4701

www.mdpi.com/journal/metals/

Article

A Study of Calcareous Deposits on Cathodically Protected Mild Steel in Artificial Seawater

Yuanfeng Yang *, James David Scantlebury † and Elena Victorovna Koroleva

School of Materials, the University of Manchester, Manchester M13 9PL, UK;
E-Mail: wilsons3ways@hotmail.com

† James David Scantlebury recently passed away on 13 July 2012.

* Author to whom correspondence should be addressed; E-Mail: yuanfeng.yang@manchester.ac.uk; Tel.: +44-161-306-2916.

Academic Editor: Hugo F. Lopez

Received: 18 December 2014 / Accepted: 15 February 2015 / Published: 12 March 2015

Abstract: Calcareous deposits were formed on steel under conditions of cathodic protection in artificial seawater at applied constant current densities ranging from 50 to 400 mA·m^{-2}. The calcareous layers were characterized using a Field Emission Gun Scanning Electron Microscope (FEG SEM) in conjunction with Energy Dispersive X-Ray Analysis (EDX), and Electrochemical Impedance Spectroscopy (EIS). At cathodic current densities of 50–100 mA·m^{-2} where corrosion was still occurring, a clear correlation existed between the iron containing corrosion product and the overlying magnesium hydroxide layer. This revealed that the mapping of magnesium rich areas on a steel surface can be used in the identification of local corrosion sites. At current densities of 150–200 mA·m^{-2}, a layered deposit was shown to occur consisting of an inner magnesium-containing layer and an outer calcium-containing layer. At current densities of 300–400 mA·m^{-2}, intense hydrogen bubbling through macroscopic pores in the deposits gave rise to cracking of the deposited film. Under such conditions deposits do not have a well-defined double layer structure. There is also preferential formation of magnesium-rich compounds near the steel surface at the early stages of polarisation and within the developing pores and cracks of calcareous deposits later on. Based on SEM/EDX investigation of calcareous depositions the impedance model was proposed and used to monitor *in situ* variations in steel corrosion resistance, and to calculate the thickness of formed deposits using the length of oxygen diffusion paths.

Keywords: calcareous deposition; corrosion; FEG SEM/EDX; EIS; artificial seawater

1. Introduction

Cathodic protection is perhaps the most powerful technique that is routinely utilised for the prevention of corrosion. The seminal study of cathodically protected mild steel using constant current was published by Humble as early as 1948 [1]. It was reported that the corrosion rate of the steel was reduced from 0.067 to 0.025 $mm \cdot y^{-1}$ when a cathodic current density increase from 0 to 100 $mA \cdot m^{-2}$ was applied; the weight loss data were based on sandblasted steel plates after one year of exposure at Kure Beach, NC. It is well established that the formation of calcareous deposits on steel contributes significantly to the effectiveness of cathodic protection and it is generally believed that calcareous deposits provide protection against corrosion by acting as a barrier to oxygen; thus preventing the cathodic reaction of oxygen reduction on the metal surface. Similar to organic paints, the calcareous deposits are poor electron conductors and cannot support the oxygen reduction on the outer surface. Additionally, like paints, they are thought to have an increased ionic resistance and to afford some degree of resistance inhibition. A considerable amount of work has already been done in understanding the mechanism formation of calcareous deposits and factors influencing this formation [2–14]. However, the effects of corrosion and the development of corrosion products under cathodic protection are reported sporadically [8,9]. More recently, publications in this area mainly deal with the examination of calcareous deposits formed on steel at constant potentials. This probably reflects the conditions employed practically for steel structures in seawater [5–14], and only a few publications consider exploiting constant current, pulse or mixed modes of polarisation [3,4,15].

As stated above, the calcareous deposit that forms on steel surfaces may be compared to a layer of electrically resistant paint. The resistance is known to increase as the layer thickens and the current automatically decreases if the voltage remains the same. Variation in electrical resistance of deposits can be monitored with the use of Electrochemical Impedance Spectroscopy (EIS), which became a popular choice of several researches examining the formation of calcareous deposits under cathodic protection at various constant potentials [10,11,14]. A particularly interesting approach was adopted by Deslouis, *et al.* [10,11] in the investigation of calcium carbonate deposits formed under cathodic protection at constant potentials applied in the range from −0.9 to −1.4 V (SCE) in calcium carbonate solution with and without magnesium salts. It is generally agreed that impedance spectroscopy is a valuable technique in monitoring *in situ* modification of steel surfaces under cathodic protection. However, the complexity of the processes occurring on the metal surface, which include reduction—oxidation (redox) together with mass transport and calcareous deposition driven by pH variation, requires a careful approach to impedance modelling.

In this study the SEM observations of cross-sectioned calcareous deposits formed on steel under cathodic protection and an EDX analysis within SEM of cross-sections are carried out in order to improve our understanding of the deposition process. It is anticipated that the distribution of Ca and Mg rich mineral deposits through the thickness of the film will provide valuable information regarding the structure and elemental composition of the films during the formation process. Knowledge of

deposit structure from direct SEM/EDX examinations will provide the solid base for selection of the impedance model in the EIS study, the aim of which is to determine the corrosion resistance of steel under conditions that consider the formation of deposits and the reduction of oxygen and water.

2. Experimental Section

2.1. Materials

The test specimens of mild steel were supplied in panels 50 × 102 × 1 mm by Q Panel Ltd. (Bolton, UK) (the composition is given in Table 1). The surfaces of the test specimens were polished using a series of sequentially finer grades of silicon carbide abrasive paper, ranging from 120 to 4000 grade (mirror finished). The test specimens were then degreased in alcohol and acetone, before final cold air drying.

Table 1. Chemical composition of mild steel.

Composition of Mild Steel					
Element	**Fe**	**C**	**Mn**	**P**	**S**
wt.%	BAL	0.08–0.13	0.3–0.6	0.04	0.05

In this work, the chemical composition chosen to prepare the artificial seawater electrolyte solution was based on the standard formulation given by Lyman and Fleming (1940; s = 3.5%) [16]. The pH of the testing solution was 7.5 ± 0.1. The temperature of the solution was on the ambient in the range of 20 ± 2 °C.

Electrochemical experiments were conducted within a three-electrode cell with the working electrode being the test specimen, the auxiliary electrode being a titanium anode coated with iridium-tantalum oxide (Mixed Metal Oxide [MMO]), supplied by BAC Corrosion control Ltd. (Telford, UK), and the reference electrode being a Saturated Calomel Electrode (SCE). Galvanostat made by Corrosion Developments (Manchester, UK) (the late Harvey Turner) was used to provide a constant current, and the value of the applied current densities could be adjusted using a built-in variable resistance. A calibrated resistor of 10,000 Ω was used in the external circuit to check the current supplied by the galvanostat.

Electrochemical Impedance Spectroscopy (EIS) was employed on the mild steel samples at different levels of galvanostatic cathodic polarization with applied current densities of 0 (the open circuit potential condition), 50, 100, 150, 200, 300 and 400 $mA \cdot m^{-2}$. During galvanostatic polarisation the variation in potential of each specimen was monitored through the duration of experiment where the initial potential values of −530, −535, −540, −550, −560, −580 and −640 mV (SCE) were followed by an increased to steady values at −690, −770, −840, −895, −950, −1000 and −1050 mV (SCE), respectively, after 1 h of polarisation. Over time, there was a further potential increase to values of −1050 and −1100 mV (SCE), which was only monitored for 300 and 400 $mA \cdot m^{-2}$ after 6 h of polarisation. Evidence of corrosion was visually observed after polarisation at 0, 50 and 100 $mA \cdot m^{-2}$. The impedance was measured at the steady potential that the specimen had immediately prior to commencing the impedance measurement. In other words, the potential was not allowed to decay back to a natural potential, as this would have removed the specimen from the specific test conditions of this study. The measurements were conducted starting initially with 6 hours immersion, then at 24 h intervals thereafter for 168 h, using an ACM (Applied Corrosion Monitoring) Gill potentiostat

(Cumbria, UK), with an inbuilt frequency response analyser over a frequency range 10,000 to 0.1 Hz. The maximum number of data readings per test was 100. All impedance spectra were analysed and modelled using Zview software (Scribner Associates Inc., Southern Pines, NC, USA).

A representative set of four samples, subjected to different levels of cathodic protection at 100, 150, 200, and 300 $mA \cdot m^{-2}$ after seven day of immersion, were cross-sectioned for examination by SEM/EDX. The current densities were chosen based on visual examination and on our previous weight loss data [17] and represent under-protected (evidence of severe corrosion), protected (trace of corrosion), well-protected (no corrosion observed) and over-protected (evidence of hydrogen evolution) steels, respectively.

Prior to cross-sectioning, each sample was carefully and slowly cut in half using a dry hand saw and the two sections were placed vertically into the middle of a polythene mould with a support. The use of two samples sections in the preparation of the SEM stub increases the length of the deposited calcareous layer and improves the reproducibility of results. An epoxy resin mixture was then poured into the mould, to a sufficient depth to completely cover the sample sections. The samples in the moulds were then placed into an oven at 60 °C for 48 h, to polymerise the resin. After polymerization and cooling, the surfaces of the cured resin blocks with the cross-sectioned samples were then polished using a series of successively finer grades of silicon carbide abrasive paper, ranging from 120 to 4000 grade. Samples were then carbon coated prior to examination in the SEM.

All SEM/EDX results presented were obtained from prepared samples, which were examined using a FEI XL-30 FEG SEM (Hillsboro, OR, USA) with an integrated RONTEC EDX facility running Quantax Esprit 1.8 analytical software (Bruker Company, Coventry, UK).

2.2. Theory and Calculations

It is well established that during the corrosion of iron or steel under neutral and alkali aqueous conditions of the marine environment, anodic metal dissolution can be supported by two major cathodic processes. Firstly, a process that consumes dissolved oxygen and generates hydroxyl ions,

$$O_2 + 2H_2O + 4e^- \rightarrow 4OH^- \quad (1)$$

and secondly, a process in which hydrogen gas is generated by the reduction of water when the potential becomes more negative as can be seen from the Pourbaix diagram [18].

$$2H_2O + 2e^- \rightarrow H_2 + 2OH^- \quad (2)$$

At potentials less negative than −950 mV (SCE), the predominant cathodic reaction is diffusion controlled oxygen reduction [19]; and in cases where the potential is more negative than −1100 mV (SCE), the risk increases of an alternative and additional cathodic reaction occurring, involving an activation controlled hydrogen evolution from the reduction of water as indicated in Equation (2) [20].

In either case, the production of hydroxyl ions results in an increase in pH of the electrolyte adjacent to the metal surface. In this way, the increase in pH in seawater will result in the precipitation of insoluble salts; *i.e.*, $CaCO_3$, $Mg(OH)_2$, and these processes can be described by the following series of reactions:

$$OH^- + HCO_3^- \rightarrow CO_3^{2-} + H_2O \quad (3)$$

$$Ca^{2+} + CO_3^{2-} \rightarrow CaCO_3 \quad (4)$$

$$Mg^{2+} + 2OH^- \rightarrow Mg(OH)_2 \quad (5)$$

These reactions collectively give rise to the formation of a calcareous film or deposit on the surface of the steel. There is general agreement in the literature that calcium carbonate precipitates at a less alkali pH compared with the pH of magnesium hydroxide precipitation [1,21]. This statement can be confirmed by simple pH calculation presented below.

The pH of calcium carbonate precipitation can be calculated from the solubility-product constant of $CaCO_3$ that is $K_{CaCO3} = [Ca^{2+}][CO_3^{2-}] = 3.8 \times 10^{-9}$ [22] at 20 °C and with knowledge of the typical concentration of Ca^{2+} in seawater of 1.123 g/1000 g of solution, which is $[Ca^{2+}] = 0.01$ M. Firstly, the concentration of CO_3^{2-}, when $CaCO_3$ begins to precipitate, can be calculated:

$$\left[CO_3^{2-}\right] = \frac{K_{CaCO_3}}{\left[Ca^{2+}\right]} = 3.8 \times 10^{-7}\,\mathrm{M} \quad (6)$$

Secondly, the concentration of OH^- required for calcium carbonate precipitation can be ascertained. The process of $CaCO_3$ precipitation occurs, when CO_3^{2-} formed during the reaction (3), where the stoichiometric concentration of OH^- being equal to the concentration of CO_3^{2-}.

Taking into consideration Equation (6), the concentration of OH^- will be:

$$\left[OH^-\right] = \left[CO_3^{2-}\right] = 3.8 \times 10^{-7}\,\mathrm{M} \quad (7)$$

Finally, the pH of seawater, during the commencement of precipitation can be calculated from the constant of water dissociation, $K_{H_2O} = \left[OH^-\right]\left[H^+\right] = 10^{-14}$:

$$[H^+] = \frac{10^{-14}}{[OH^-]} = 2.63 \times 10^{-8}\,\mathrm{M} \quad (8)$$

So the pH, when calcium carbonate begins to precipitate is $pH = -\log [H^+] = 7.58$, the value being lower than the pH of normal seawater. This result apparently indicates that $CaCO_3$ is readily precipitated in normal seawater without the assistance of cathodic protection. However, assuming a different value for activity coefficients, the calculations give a pH of 8.7 for precipitation of $CaCO_3$. This appears to be more consistent with the situation that actually occurs in practice.

Similarly in order to precipitate $Mg(OH)_2$ with the solubility-product constant $K_{Mg(OH)2} = 6 \times 10^{-10}$ [22] and the concentration of $[Mg]^{2+} = 0.053$ M, which is a typical concentration of $[Mg]^{2+}$ in seawater (5.07 g/1000 g solution), a significantly higher pH is required if we compare this with the pH necessary for $CaCO_3$ precipitation to occur. The magnesium hydroxide precipitates according to the reaction (5) with $K_{Mg(OH)_2} = \left[Mg^{2+}\right]\left[OH^-\right]^2$.

The concentration of OH^- when $Mg(OH)_2$ precipitates can be calculated from $K_{Mg(OH)2}$ and will be:

$$\left[OH^-\right] = \sqrt{\frac{K_{Mg(OH)_2}}{\left[Mg^{2+}\right]}} = \sqrt{\frac{6 \times 10^{-10}}{5.3 \times 10^{-2}}} = 1.06 \times 10^{-4}\,\mathrm{M} \quad (9)$$

The $[H^+]$ at the commencement of $Mg(OH)_2$ precipitation will be:

$$[H^+] = \frac{10^{-14}}{[OH^-]} \approx 10^{-10}\,\mathrm{M} \quad (10)$$

So the pH for precipitation of $Mg(OH)_2$ is around 10.

Previously, Engell and Forchhammer [23] predict that at 20 °C, $Mg(OH)_2$ would be precipitated at pH 9.7 and $CaCO_3$ at pH 7.27.

When steel is under cathodic protection in seawater, the pH near the steel surface slowly becomes more alkaline due to oxygen reduction [2] and the deposition of calcium carbonate is expected to occur first. In previous studies [3,5,6,17] it was demonstrated that the compound that is initially precipitated next to the iron-containing corrosion products is possibly brucite ($Mg(OH)_2$), and not calcium-rich aragonite (calcium carbonate, $CaCO_3$). The presence of brucite in the vicinity of iron hydroxides might be explained by the co-precipitation of brucite during the formation of corrosion products when steel corrodes. The possibility of co-precipitation is based on the work by Packter and Derby [24] who established and examined the mechanisms of co-precipitation of magnesium and iron hydroxides from aqueous solution using potentiometric titration.

Iron hydroxide precipitates at a significantly lower pH compared to that of $CaCO_3$ and this pH can be calculated from the solubility-product constant [22], $K_{Fe(OH)_3} = 6.3\times10^{-38}$ of ironhydroxide and the reaction of hydroxide formation $Fe^{3+} + 3OH^- = Fe(OH)_3$, assuming that theconcentration of $[Fe^{3+}] = 0.01$ M (the concentration of Fe^{3+} has been chosen to be similar to the concentration of Ca^{2+} in seawater), the concentration OH^- and H^+ during iron hydroxide precipitation will be:

$$\left[OH^-\right] = \sqrt[3]{\frac{K_{Fe(OH)_3}}{\left[Fe^{3+}\right]}} = \sqrt[3]{\frac{6.3\times10^{-38}}{10^{-2}}} = 1.8\times10^{-12}\,\mathrm{M} \tag{11}$$

$$[H^+] = \frac{10^{-14}}{\left[OH^-\right]} = 5.4\times10^{-3}\,\mathrm{M} \tag{12}$$

The pH for precipitation of $Fe(OH)_3$ is pH = −log $[H^+]$ = 2.26.

For the situation where iron (III) hydroxides will be formed due to corrosion of steel in oxygenated seawater, $Mg(OH)_2$ might be precipitated together with iron (III) hydroxides at a pH as low as 2.26, and hence well before precipitation of $CaCO_3$.

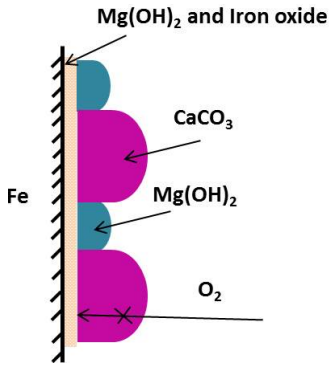

Figure 1. Schematic diagram of calcareous film formation on mild steel during cathodic protection in artificial seawater [25].

The above calculations are necessary to support the explanation of the formation of the thin $Mg(OH)_2$ inner layer in the presence of corrosion. This occurs during the early stages of calcareous deposition and within the pores of the deposits. A schematic diagram [25] that illustrates the process of

calcareous film formation on a cathodically protected mild steel surface in seawater is presented in Figure 1. The diagram takes in consideration partial steel dissolution within the areas where $Mg(OH)_2$ co-precipitates with corrosion products of iron.

3. Results and Discussion

In conventional cathodically protected submerged sea structures, the recommended optimum range of protection potential is between −900 and −1050 mV (Ag/AgCl) [26] or −950 and −1100 mV (SCE) measured against a calomel reference electrode. The system is considered to be under-protected when potential values are above −800 mV (Ag/AgCl) or −850 mV (SCE) and over-protected with potential values below −1150 mV (Ag/AgCl) or −1200 mV (SCE). It is common towards the end of the service life of these structures, or during an interruption of cathodic protection, that the potential becomes higher than −850 mV (SCE) leading to increased levels of corrosion. In this work the constant current polarisation is used deliberately to allow the development of corrosion products during the early stages of cathodic protection and, in some cases, through the entire polarisation. For all levels of polarisation the initial potentials are significantly above the recommended values, ranging between −530 and −640 mV (SCE). The potentials are reduced below −850 mV (SCE) after 1 h of polarisation at 150, 200, 300 and 400 $mA \cdot m^{-2}$. However steel remains under-protected at 50 and 100 $mA \cdot m^{-2}$ during the first 168 h and beyond.

3.1. Examination of Calcareous Deposits by SEM with EDX

The SEM micrographs and corresponding overlaid Energy Dispersive X-Ray Analysis (EDX) element distribution maps for Mg, Ca and Fe of the cross-sectioned samples subjected to the four different current densities are presented in Figure 2. The dark green area is magnesium containing, the pink area is calcium containing, and the red region is base iron metal or iron oxide.

The deposit layers formed at any level of cathodic protection are well defined, intact and adherent both to steel substrate and to each other (Figure 2). The variation in total thickness of deposition is in the range of 30 and 50 μm and is observed to a larger extent along the steel surface compared to that of the level of cathodic protection. Furthermore, the magnesium containing layers are frequently found to be associated with iron. The magnesium-containing layer is clearly present above corrosion products of iron (Figure 2a) or above the metal surface that has some degree of hydrated iron oxide formed during steel corrosion (Figure 2b).

For under protected steel with deposition at lower current density of 100 $mA \cdot m^{-2}$ and the steady potential of around −840 mV (SCE) the presence of local areas filled with corrosion products is a clear indication of the occurrence of anodic iron dissolution, where the precipitation of iron hydroxides is inevitable at a pH of 7.5. The presence of a relatively thick layer (thickness of about 30 μm) containing magnesium above iron hydroxides suggests co-precipitation of magnesium and iron hydroxides at localised sites on the steel surface. The presence of magnesium rich areas reveals sites of active steel dissolution when cathodically under-protected conditions are applied (Figure 2a). Mapping the steel surface for the presence of magnesium can be used in assessing corrosion damage.

For protected steel with deposition at applied current densities of 150 and 200 $mA \cdot m^{-2}$ with potentials of around −895 and −950 mV (SCE), respectively, the thin magnesium containing layer

(thickness of about 10 μm) with incorporated iron is observed near the metal surface with the thick layer of calcium rich compound (thickness of about 30 and 50 μm, respectively) formed above it (Figure 2b,c). The presence of the magnesium-containing layer near the metal indicates a small level of iron dissolution, which leads to the formation of a mixture of iron and magnesium hydroxides. This occurs prior to the protection provided by calcium carbonate, which deposits when the pH increases to above 8.7. Additionally, the magnesium rich compound only is observed within occasional pores indicating a significant pH increase above 10 and preferential precipitation of magnesium hydroxide within those pores during the formation of calcareous deposit layers. The high pH suggests that the reduction of oxygen proceeds at the bottom of the pore and associated mass transport processes lead to a fast pH increase compared with the pH at the deposit-seawater interface. Defined sites of oxygen reduction during the formation of layers usually correspond to areas of initial anodic dissolution of the steel, since a large amount of iron rich compound is present at the bottom of the pore (Figure 2a). This evidence is used in developing the impedance model, where "active" pores propagate through both layers of deposit and provide sites for steel corrosion, oxygen reduction and mass transport of active species. Some magnesium rich areas can be observed within the bulk of calcium containing layer (Figure 2c). The latter can be explained by cross-sectioning the large convoluted pore away from the surface of the metal; this reveals isolated areas of magnesium-rich compound within the calcium carbonate.

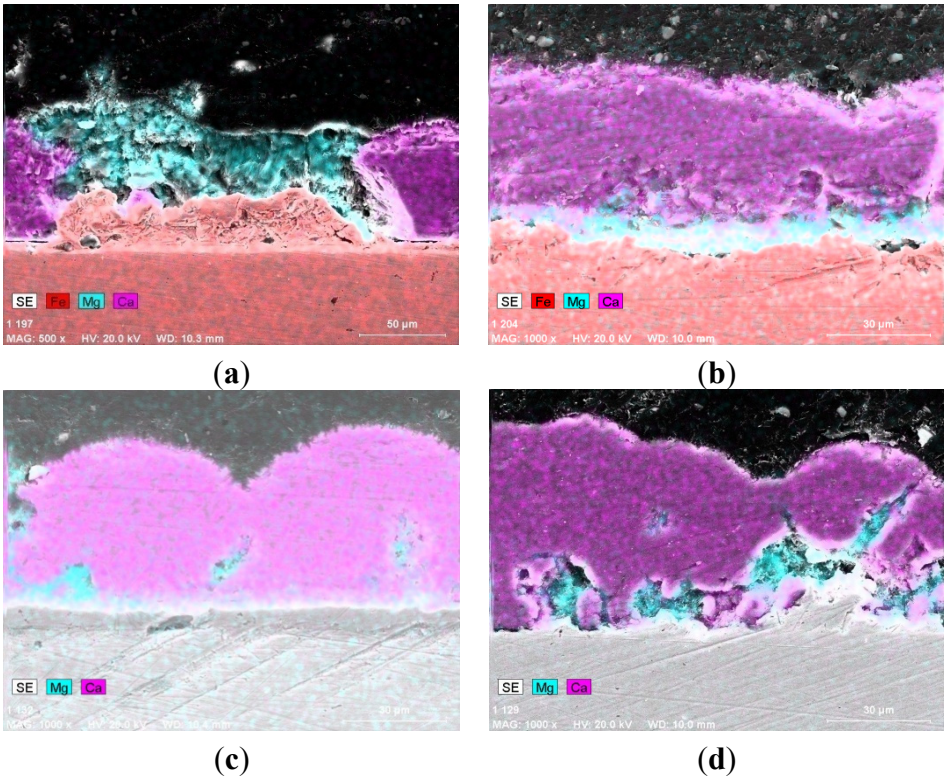

Figure 2. Secondary electron micrographs and corresponding overlaid Energy Dispersive X-Ray Analysis (EDX) element distribution maps for Fe, Mg and Ca of cross-section of calcareous deposit formed after 144 h immersion in seawater at applied current densities of: (**a**) 100 mA·m^{-2}; (**b**)150 mA·m^{-2}; (**c**) 200 mA·m^{-2}; (**d**) 300 mA·m^{-2}.

For steel subjected to 300 $mA \cdot m^{-2}$ and the potentials of −1050 mV (SCE) (Figure 2d), a high level of alkalization near the metal surface is inevitable and is associated with the commencement of hydrogen evolution, which proceeds on the steel at the beginning of polarisation, and within the pores and cracks of the deposits after their formation. At this stage hydrogen evolves in the form of microscopic bubbles, as there is no detachment of the deposits. Under such conditions deposits have a not so well defined double layer structure with a preferential formation of a magnesium-rich compound near the surface at the early stages of polarisation, and within the developing pores and cracks of calcareous deposition later on.

Currently, the presence and formation of a thin inner layer of magnesium hydroxide on the steel, under cathodic protection, is attributed to a high level of alkalisation (above 10) near the surface due to the reduction of oxygen and at very low potentials, due to the process of water reduction [2,5,6,15]. This statement is very well justified for cathodically protected steel, which has no evidence of corrosion. In a situation when corrosion proceeds in seawater, the hydrolysis of water results in the formation of iron (II and III) hydroxysalts, more commonly known as green rust [8,9,27]. It is a known fact that the formation of corrosion products leads to acidified conditions near the surface of corroding steel promoting further dissolution of iron. For example, the measurement of pH near the surface of a corroding sea wreck indicated a pH variation in the range of 4.2–7.9 while seawater had an average pH of 8.4 [28].

This work demonstrated the presence of an inner magnesium-containing layer, together with corrosion products, and the ready formation of magnesium hydroxide above corrosion products within the pores of the deposit under all levels of cathodic polarisation from 50 to 400 $mA \cdot m^{-2}$. This can only be explained by the initial co-precipitation of magnesium and iron hydroxides at a pH lower than expected, and below a pH of 7.3 (commencement of calcium carbonate precipitation). The post-precipitation of magnesium hydroxide is possible over mixed magnesium-iron hydroxysalts at later stages of precipitation. Once precipitated, the magnesium hydroxide is only slightly soluble and does not re-dissolve [29]. Co-precipitation of magnesium and iron (III) hydroxides is known at pH as low as 3.5 [24] and since ionic radiuses of magnesium (II) and iron (III) are similar (0.64 Å), it is more likely the mechanism of co-precipitation is inclusion, which represents the most efficient co-precipitation method that produces mixed crystals [30]. It was recently proposed to use magnesium hydroxide in the mining industry for the removal of acidity and metals from drainage water [31]. The latter paper illustrated an increased rate for oxidation of iron (II) to iron (III) and the precipitation of iron (III) hydroxide at a pH of around 5.5–6 on the addition of magnesium hydroxide to water. Equilibrium between soluble/insoluble phases of magnesium hydroxide, which supported oxidation and precipitation of iron, is directly relevant to the mechanism of formation of calcareous deposits on steel under cathodic protection.

Overall, the SEM and EDX results obtained from samples under all cathodic protection levels revealed that the deposits were composed of two layers (inner layer was magnesium-rich whilst the outer layer was calcium-rich) with a clear boundary and occasional pores running through the layers filled with a magnesium-rich compound providing sites for reduction—oxidation and associated mass transport. These results were in agreement with previous findings [3,5,6,15] and provided the basis for the design of equivalent circuits utilised during analysis and the modelling of impedance data.

3.2. Study of the Calcareous Deposit Formation by Electrochemical Impedance Spectroscopy

A double-layered structure of deposition, with a limited amount of "active" pores, is used for modelling our system. The electrochemical behaviour of mild steel under conditions of cathodic protection with on-going electrochemical anodic and cathodic processes is based partly on the models proposed by Deslouis [10,11] and Chung [32].

The Deslouis model had already been used for the interpretation of corrosion resistance of mild steel under cathodic protection in the presence of a calcareous deposition, which partially covered the surface (Figure 3a). In this model the properties of the continuous film were represented by a parallel combination of film capacitance and resistance, C_f and R_f, respectively, together with a charge transfer resistance R_{ct}, and a double layer capacitor C_{dl}, and collectively these represented the corrosion processes proceeding at the metal interface. The aforementioned work also introduced an additional parallel combination of R_d and C_d to mimic the uncovered areas (pores) of the surface. However, this model did not take into consideration the formation of corrosion product within the film.

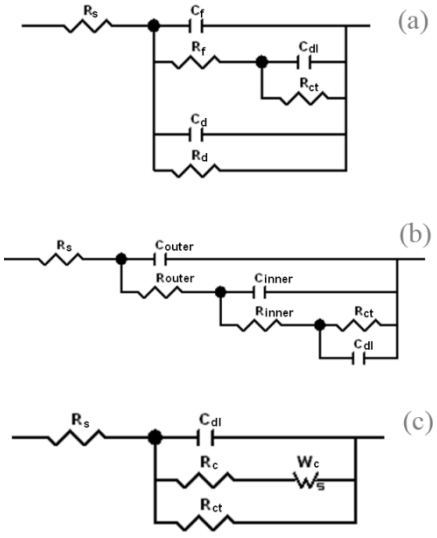

Figure 3. Equivalent circuits of the models used previously: (**a**) the equivalent circuit of original Deslouis's model [3]; (**b**) the equivalent circuit of Chung's model [32]; (**c**) the equivalent circuit of Barchiche and Deslouis's model [14].

The model introduced by Chung [32] had been used for the description of the corrosion resistance of an anodic porous coating formed during spark anodising on zinc in NaCl solution. According to this model the coating film consisted of outer and inner layers where the pores of the inner layer were filled with corrosion products formed during metal dissolution at the interface (Figure 3b). This model, or a modification of it, was considered as a possibility to explain our data.

The original Deslouis [10] model did not consider the occurrence of cathodic electrochemical processes, which clearly should have a significant contribution to the impedance of cathodically protected steel. A second and subsequent model from Deslouis and co-workers [14] showed that the corrosion filmed on mild steel under natural immersion conditions in NaCl solutions can be modelled by equivalent circuits with anodic and cathodic branches being in parallel with a double layer capacitor C_{dl}. The anodic branch was represented by the anodic charge transfer resistance R_{ct}, and the cathodic

branch was under mixed control and comprised the resistance of the charge transfer reaction R_c, together with a diffusion limited Warburg impedance W_c (Figure 3c).

Analysis of our EIS data reveals that in most cases the impedance spectra consists of three semicircles with two semicircles of relatively small diameters probably associated with the properties of the calcareous film observed at higher frequencies, and one semicircle of large diameter associated with dissolution (corrosion of steel) followed by a straight line turning into a semicircle at lower frequencies. Figure 4 gives a typical example for a Nyquist plot obtained for a sample using a current density of 150 $mA \cdot m^{-2}$ over 72 h immersion in artificial seawater together with a modelling curve and a schematic diagram of the model proposed in Figure 5. Schematic diagram is based on the total impedance of the system presented by equation:

$$Z(\omega) = R_s + [j\omega C_{outer} + (R_{outer} + \{j\omega C_{inner} + [R_{inner} + (j\omega C_{dl} + R_a^{-1} + W_c^{-1})^{-1}]^{-1}\}^{-1})^{-1}]^{-1} \quad (13)$$

when $\omega \rightarrow 0$ $Z(\omega) = R_s + R_{outer} + R_{inner} + (R_a W_{C\text{-}R})/(R_a + W_{C\text{-}R})$.

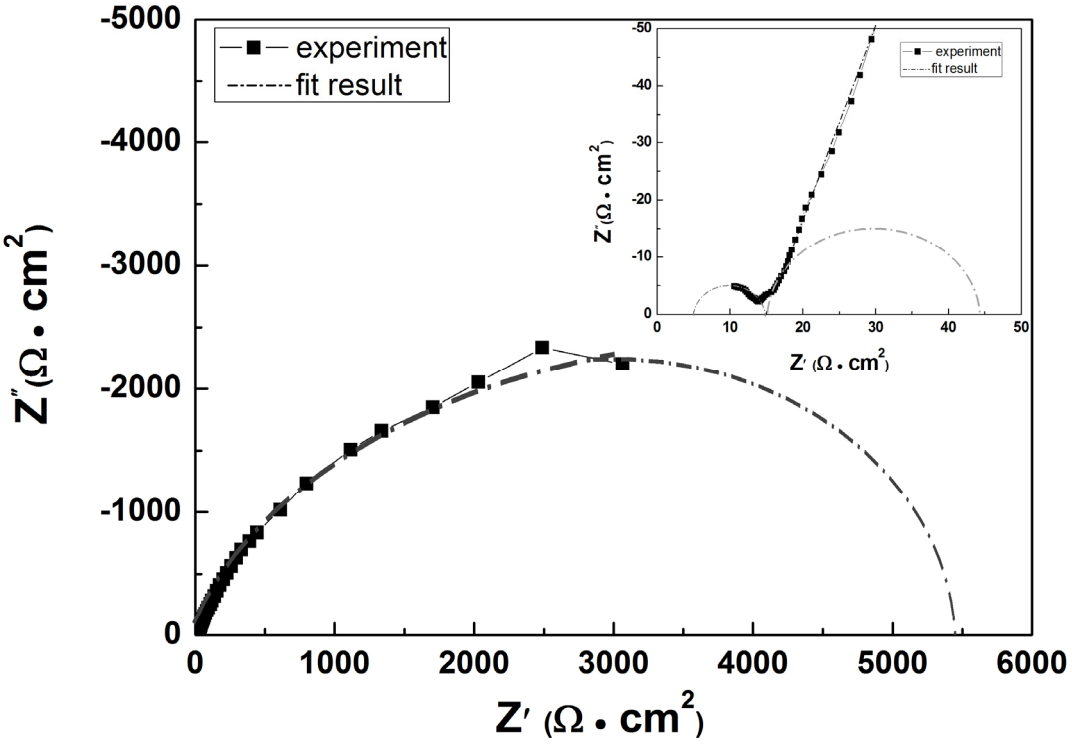

Figure 4. The Nyquist plot obtained for a mild steel sample at 150 $mA \cdot m^{-2}$ over 72 h immersion in artificial seawater and plotted together with modelling curve based on equivalent circuit of Figure 5.

From Figure 5, our model comprises a solution resistance R_s and a two layered deposit. The outer layer L_{outer} is a calcium rich layer; and the inner layer L_{inner} is a magnesium and iron rich layer. The outer layer L_{outer} is considered to be porous and is characterised by a parallel combination of a capacitor C_{outer} which is directly associated with the thickness of the calcium containing deposits, and a pore resistance R_{outer} which is defined by the resistance of all of the pores. The inner compact layer L_{inner} and the corroding steel are introduced into the equivalent circuit, which is in series with R_{outer}. The L_{inner} is also characterized by a parallel combination of a capacitor C_{inner} that determined by thickness of inner layer and a resistance R_{inner}, which determined the ionic path to the metal substrate. The R_{inner} is

different from R_{outer} by the value of conductivity and the true area of conduction. The corroding interface is characterised by a parallel combination of a double layer capacitor C_{dl}, charge transfer anodic resistance R_a, and a finite-length impedance of diffusion W_c, which represents the cathodic process. To simplify our already complex equivalent circuit, the resistance of cathodic charge transfer reaction is considered small and the system is totally mass transport controlled unlike the model used by Bonnel (see Figure 3c). The quality of our data fit (Figure 4) clearly shows the validity of the model chosen and as an example the best fit result for equivalent circuit elements at 150 $mA \cdot m^{-2}$ is presented in Table 2.

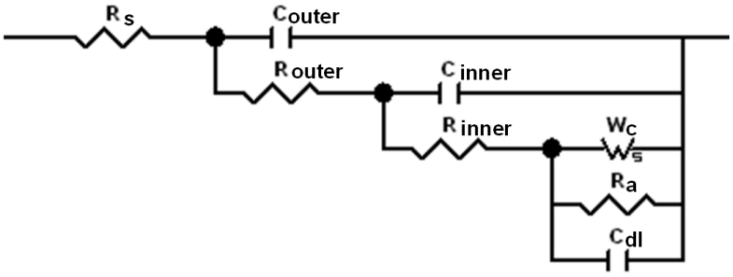

Figure 5. Equivalent circuit for mild steel in artificial seawater under cathodic protection, where R_s—resistance of the electrolyte; C_{outer}—capacitor associated with calcium containing layer; R_{outer}—resistance associated with ionic conduction through the occasional pores; C_{inner}—capacitor associated with magnesium containing layer; R_{inner}—resistance associated with ionic conduction through this layer; C_{dl}—capacitor of double layer on metal/deposit interface; R_a—anodic charge transfer resistance; W_c—cathodic finite-length Warburg impedance.

Analysis of equivalent circuit elements for the applied current densities (as an example see Table 2) indicates that the contribution of the inner and outer layer to the impedance of the system is less than 1% compared to the contribution of impedance associated with diffusion of cathodic active species through the layers and the impedance of anodic dissolution on the metal-deposit interface. Therefore the analysis of impedance data is focused on diffusion and anodic dissolution. The cathodic processes on the steel surface are described by the open finite-length Warburg impedance (open Warburg element) since diffusion of the electrochemically active species (oxygen) is thought to be a limiting stage of the cathodic process. The oxygen concentration near the metal interface is fixed and constant due to the slow diffusion of oxygen through the deposits of active pores. The open Warburg element is characterised by two parameters a $W_{C\text{-}R}/\Omega \cdot cm^2 \cdot s^{-0.5}$ and $W_{C\text{-}T}/s^{-0.5}$. The equation for open Warburg element is:

$$W_c(\omega) = W_{C-R} \times \tanh\left(W_{C-T} \times (j\omega)^{0.5}\right) \Big/ \left(W_{C-T} \times (j\omega)^{0.5}\right) \quad (14)$$

The open Warburg element on Nyquest plot will be a straight line with a 45° gradient at high frequencies ($\omega > 2/W_{C\text{-}T}^2$) which will turn to a semicircle at very low frequencies, with ω approaching to 0. The $W_{C\text{-}R}$ parameter is the Warburg coefficient, which defines diffusion resistance and can be used to calculate a diffusion coefficient for the mobile species within the deposits. The $W_{C\text{-}T}$ parameter is a time constant which defines the time required for the species to diffuse through the deposits:

$W_{C\text{-}T} = h \times D^{-0.5}$, where h is the thickness of deposit and D is a diffusion coefficient of active species. The data, which has been extracted from our model, show an excellent fit with the open Warburg element.

Table 2. Best fit results for equivalent circuit elements at applied current density of 150 $mA \cdot m^{-2}$.

Immersion Time/h	6	24	48	72	96	120	144	168
$R_s/\Omega \cdot cm^2$	12.3	13.6	12.1	9	10.5	9.8	10.8	11.8
$C_{outer}/F \cdot cm^{-2}$	2.1×10^{-6}	1.1×10^{-6}	0.6×10^{-6}	2.4×10^{-6}	3.4×10^{-6}	2.6×10^{-6}	3.2×10^{-6}	1.3×10^{-6}
$R_{outer}/\Omega \cdot cm^2$	7.4	10.7	14.6	6	5.4	6.8	6.3	9.8
$C_{inner}/F \cdot cm^{-2}$	43×10^{-6}	52×10^{-6}	45×10^{-6}	43×10^{-6}	35×10^{-6}	37×10^{-6}	34×10^{-6}	36×10^{-6}
$R_{inner}/\Omega \cdot cm^2$	58	55	67	28	34	48	41	61
$W_{C\text{-}R}/\Omega \cdot cm^2$	7400	7400	8900	7900	9000	10,000	8800	7800
$W_{C\text{-}T}/s^{-0.5}$	2.8	4.4	4.6	3.6	4.3	5	5	3.5
$R_a/\Omega \cdot cm^2$	100,400	130,000	15,400	14,900	13,800	14,600	22,200	14,300
$C_{dl}/F \cdot cm^{-2}$	26×10^{-6}	37×10^{-6}	28×10^{-6}	32×10^{-6}	24×10^{-6}	25×10^{-6}	25×10^{-6}	23×10^{-6}

The variation of cathodic parameters $W_{C\text{-}R}$ and $W_{C\text{-}T}$ over immersion time at different current densities is given in Tables 3 and 4 and the variation of anodic charge transfer resistance, R_a is presented in Table 5. Generally, the Warburg coefficient $W_{C\text{-}R}$ increases with current density up to 200 $mA \cdot m^{-2}$ followed by a significant reduction for current densities 300 $mA \cdot m^{-2}$ and above. This behaviour coincides with reduction in $W_{C\text{-}T}$ values (Tables 3 and 4). The R_a increases with an increase in applied cathodic current density. The conditions (current density and immersion time) where anodic charge transfer resistances R_a are very high and above 100,000 $\Omega \cdot cm^2$ (highlighted in the grey in Table 5), anodic iron dissolution is negligible or impossible. In the latter case the electrochemical potential of the system is below the redox potential of iron. The resistance, R_a of over 10,000 $\Omega \cdot cm^2$ has been arbitrarily chosen as a measure of full cathodic protection. It was confirmed that the anodic charge transfer resistance is clearly associated with iron dissolution, and closely follows weight loss experiments used in the calculation of corrosion rate [17]; as the resistance increases so corrosion rate decreases.

Table 3. Values of cathodic diffusion resistance $W_{C\text{-}R}/\Omega \cdot cm^2 \cdot s^{-0.5}$ with immersion time at different applied current densities.

Immersion Time/h	6	24	48	72	96	120	144	168
50 $mA \cdot m^{-2}$	3000	5800	4800	4300	4300	3700	2100	3300
100 $mA \cdot m^{-2}$	3100	5200	6900	8100	6800	7300	7500	7900
150 $mA \cdot m^{-2}$	7400	7400	8900	7900	9000	10,000	8800	7800
200 $mA \cdot m^{-2}$	6900	10,600	8800	7300	8700	11,100	10,000	9000
300 $mA \cdot m^{-2}$	4100	4000	3300	2400	2600	2200	2000	1800
400 $mA \cdot m^{-2}$	3100	2000	2500	1400	1100	1400	1000	1000

Table 4. Values of $W_{C\text{-}T}/s^{-0.5}$ with immersion time at different applied current densities.

Immersion Time/h	6	24	48	72	96	120	144	168	Average $W_{C\text{-}T}$ between 24 and 168 h
50 mA·m^{-2}	1	3	3.3	3.2	3.6	3.3	4	3.2	3.4
100 mA·m^{-2}	3.3	1.7	3.3	2.8	2.3	3	3.7	2.2	2.7
150 mA·m^{-2}	2.8	4.4	4.6	3.6	4.3	5	5	3.5	4.3
200 mA·m^{-2}	2.1	7	4.3	3.7	3.6	5.8	7.3	8.6	6.2
300 mA·m^{-2}	1.4	2.2	1.4	0.6	1.1	0.7	0.8	0.8	1.1
400 mA·m^{-2}	2.2	1.7	1.4	0.6	0.6	0.8	0.6	0.6	0.9

Table 5. Values of anodic charge transfer resistance $R_a/\Omega\cdot cm^2$ with immersion time at different applied current densities.

Immersion Time/h	6	24	48	72	96	120	144	168
50 mA·m^{-2}	3100	4000	3500	3100	5700	3100	2400	2600
100 mA·m^{-2}	58,700	20,000	8000	9600	6600	8800	10,000	20,000
150 mA·m^{-2}	100,400	130,000	15,400	14,900	13,800	14,600	22,200	14,300
200 mA·m^{-2}	1.15×10^{15}	2.8×10^{10}	34,600	10,300	23,800	12,000	25,000	30,000
300 mA·m^{-2}	1×10^{20}	1×10^{20}	1×10^{20}	1×10^{20}	1×10^{20}	1×10^{20}	1×10^{20}	1×10^{20}
400 mA·m^{-2}	1×10^{20}	1×10^{20}	1×10^{20}	1×10^{20}	1×10^{20}	1×10^{20}	1×10^{20}	1×10^{20}

For under-protected steel with an applied current density of 50 mA·m^{-2}, oxygen diffusion, oxygen reduction and iron dissolution proceed simultaneously. The values of R_a are fairly low, being between 2400–5700 $\Omega\cdot cm^2$, the values of $W_{C\text{-}R}$ are in the range of 2100–5800 $\Omega\cdot cm^2\cdot s^{-0.5}$ and $W_{C\text{-}T}$ are between 1 and 4 $s^{-0.5}$, which is relatively high (Tables 3–5). High values of $W_{C\text{-}T}$ indicate that the oxygen reduction process needs to be considered in modelling at low current densities when the system is probably under mixed activation/diffusion control.

Increasing the current density to 100 mA·m^{-2} results in slow steady increase in $W_{C\text{-}R}$ from 3100 to 8100 $\Omega\cdot cm^2\cdot s^{-0.5}$ during first 72 h immersion, then $W_{C\text{-}R}$ reduce to 6800 $\Omega\cdot cm^2\cdot s^{-0.5}$ after a further 24 h immersion (total 96 h), before increasing again to almost 8000 $\Omega\cdot cm^2\cdot s^{-0.5}$ after 168 h immersion. The pattern of increasing Warburg coefficient followed by sudden decrease and subsequent increase is most likely explained by the slow thickening of deposited layers during first 72 h followed by sudden detachment of local regions of calcareous film at 96 h with further re-growth in the remaining 168 h. Detachment is possible due to the slow formation of the deposit under a relatively low current density. The thickness of layers is 12 μm and was calculated from average $W_{C\text{-}T}$ of 2.7 $s^{-0.5}$ and the diffusion path of the active specie (oxygen), with the diffusion coefficient of oxygen $D = 2.25 \times 10^{-5} cm\cdot s^{-1}$ [33]. Interestingly, the R_a varied between 6600 and 58,700 $\Omega\cdot cm^2$, where the lowest value of 6600 $\Omega\cdot cm^2$ is observed after 96 h of immersion, indicating an increased rate of corrosion. This further confirms possible detachment of the protected film at that point.

The impedance data for the two intermediate current densities of 150 and 200 mA·m^{-2} show excellent corrosion resistance with R_a being above 10,300 $\Omega\cdot cm^2$ for the entire immersion time. The weight loss results clearly show that the metal dissolution is negligible at these current densities. Initially, after 6 h of immersion, the $W_{C\text{-}R}$ values is 7400 and 6900 $\Omega\cdot cm^2\cdot s^{-0.5}$, respectively, compared to 3100 $\Omega\cdot cm^2\cdot s^{-0.5}$ observed at 100 mA·m^{-2}. This indicates a relatively fast film formation under such conditions. The film continues to grow over time achieving the maximum value of 11,000 $\Omega\cdot cm^2\cdot s^{-0.5}$.

The average diffusion paths of oxygen calculated from the average $W_{C\text{-}T}$ values for 150 $mA \cdot m^{-2}$ and 200 $mA \cdot m^{-2}$ are 20 μm and 29 μm, respectively. The calculation with use of $W_{C\text{-}T}$ values (5 $s^{-0.5}$ and 8.6 $s^{-0.5}$) close to the end of immersion time (144 h and 168 h) results in oxygen diffusion paths of 24 μm and 41 μm, respectively, which are very close to the thickness of deposits measured directly from SEM cross-section (Figure 2b,c).

For the steel under cathodic protection of 300 and 400 $mA \cdot m^{-2}$, the values of anodic resistance R_a tend to infinity, indicating that the anodic dissolutions of iron has ceased. This conclusion is in agreement with values of cell potential of −1050 mV (SCE) at 300 $mA \cdot m^{-2}$ and −1100 mV (SCE) at 400 $mA \cdot m^{-2}$, respectively, those potentials being significantly below the redox potential of iron. The $W_{C\text{-}R}$ values are reduced and are in range of 1000 and 4100 $\Omega \cdot cm^2 \cdot s^{-0.5}$. The oxygen diffusion paths, calculated from the average $W_{C\text{-}T}$ values for 300 $mA \cdot m^{-2}$ and 400 $mA \cdot m^{-2}$, are 0.5 μm and 0.4 μm, respectively. The significantly reduced cathodic parameters are a result of neglecting the commencement of hydrogen evolution in the impedance model where an additional resistance assigned to activation controlled water reduction should be introduced parallel to the Warburg impedance.

The modelling of impedance data used in this work allows successful calculation of corrosion resistance of the steel for wide range of cathodic protection levels covering under-protected, fully protected and over-protected conditions. Additionally the thickness of the deposited layers is calculated reliably for steel under fully protected conditions of cathodic protection.

4. Conclusions

It is confirmed that calcareous deposits are formed under all conditions of cathodic protection, e.g., partly protected, fully protected and protected with some level of hydrogen evolution.

The formation of deposits is assisted by the pH increase and begins with the co-precipitation of magnesium and iron hydroxides followed by calcium carbonate, producing a double-layered deposition. At later stages of calcareous deposit formation under conditions of partial protection the magnesium hydroxide precipitates within the pores and cracks above corrosion products. The ability of magnesium hydroxide to precipitate together with corrosion products formed in oxygenated seawater can be used to assess the level and location of corrosion damage of under-protected installations.

The variation in corrosion resistance of cathodically protected steel is assessed *in situ* by electrochemical impedance spectroscopy with modelling based on the knowledge of elemental distribution within the deposition obtained from SEM/EDX investigations. It is found that the contribution of deposit layers to total impedance of the system is less than 1% compared with the contribution of oxygen diffusion through the layers, and the contribution of metal resistance to dissolution. Resistance to dissolution (the anodic charge transfer process of iron dissolution) is steadily increased with the level of cathodic protection and becomes infinitely large at high current densities; a resistance over 10,000 $\Omega \cdot cm^2$ provides full cathodic protection. Open finite length diffusion Warburg impedance is employed in assessing diffusion of oxygen through the deposit layers. The length of the oxygen diffusion paths has been calculated and correlated well with an average thickness (30–50 μm) of deposits formed under conditions of full cathodic protection and measured directly from SEM micrographs.

Acknowledgments

This paper is written in memory of our co-author, colleague, friend and teacher James David Scantlebury. Yuanfeng Yang would like to thank the Dorothy Hodgkin Postgraduate Award (DHPA) for provision of a research studentship during the PhD studies. The University of Manchester is also thanked for providing an EPSRC PhD Plus Award to Yuanfeng Yang during 2010.

Author Contributions

Yuanfeng Yang designed and conducted all the experiments, with the supervisory assistance of James David Scantlebury. Elena Victorovna Koroleva examined the experimental results and assisted with the analysis. All authors have contributed to discussing and revising the article script.

Conflicts of Interest

The authors declare no conflict of interest.

References

1. Humble, R.A. Cathodic protection of steel in sea water with magnesium anodes. *Corrosion* **1948**, *74*, 358–379.
2. Wolfson, S.L.; Hartt, W.H. An initial investigation of calcareous deposits upon cathodic steel surfaces in sea water. *Corrosion* **1981**, *37*, 70–76.
3. Luo, J.S.; Lee, R.U.; Chen, T.Y.; Hartt, W.H.; Smith, S.W. Formation of calcareous deposits under different modes of cathodic polarization. *Corrosion* **1991**, *47*, 189–196.
4. Li, C.; Du, M.; Qiu, J.; Zhang, J. Influence of temperature on the protectiveness and morphological characteristics of calcareous deposits polarized by Galvanostatic mode. *Acta Metall. Sin.* **2014**, *24*, 131–139.
5. Barchiche, C.; Deslouis, C.; Gil, O.; Refait, P.; Tribollet, B. Characterization of calcareous deposits by electrochemical methods: Role of sulphates, calcium concentration and temperature. *Electrochim. Acta* **2004**, *49*, 2833–2839.
6. Barchiche, C.; Deslouis, C.; Gil, O.; Joiret, S.; Refait, P.; Tribollet, B. Role of sulphate ions on the formation of calcareous deposits on steel in artificial seawater; the formation of Green Rust compounds during cathodic protection. *Electrochim. Acta* **2009**, *54*, 3580–3588.
7. Zakowski, K.; Szocinski, M.; Narozny, M. Study of the formation of calcareous deposits on cathodically protected steel in Baltic sea water. *Anti-Corros. Methods Mater.* **2013**, *60*, 95–99.
8. Refait, P.; Jeannin, M.; Sabot, R.; Antony, H.; Pineau, S. Electrochemical formation and transformation of corrosion products on carbon steel under cathodic protection in seawater. *Corros. Sci.* **2013**, *71*, 32–36.
9. Refait, P.; Jeannin, M.; Sabot, R.; Antony, H.; Pineau, S. Corrosion and cathodic protection of carbon steel in the tidal zone: Products, mechanisms and kinetics. *Corros. Sci.* **2015**, *90*, 375–382.
10. Deslouis, C.; Festy, D.; Gil, O. Characterization of calcareous deposits in artificial seawater by impedance techniques—I./Deposit of $CaCO_3$ in the absence of $Mg(OH)_2$. *Electrochim. Acta* **1998**, *43*, 1891–1901.

11. Barchiche, C.; Deslouis, C.; Festy, D.; Gil, O.; Refait, P.; Touzain, S.; Tribollet, B. Characterization of calcareous deposits in artificial seawater by impedance techniques—II./Deposit of $CaCO_3$ in the presence of Mg(II). *Electrochim. Acta* **2003**, *48*, 1645–1654.
12. The effects of surface films on cathodic protection. Available online: http://www.jcse.org/viewpreprint.php?vol=9&pap=3 (accessed on 11 March 2015).
13. Leeds, S.S.; Cottis, R.A. An investigation into the influence of surface films on the mechanism of cathodic protection. In Proceedings of the NACE Corrosion Conference, San Diego, CA, USA, 12–16 March 2006.
14. Bonnel, A.; Dabosi, F.; Deslouis, C.; Duprat, M.; Keddam, M.; Tribollet, B. Corrosion study of a carbon steel in neutral chloride solutions by impedance techniques. *J. Electrochem. Soc.* **1983**, *4*, 753–762.
15. Zamanzade, M.; Shahrabi, T. Improvement of corrosion protection properties of calcareous deposits on carbon steel by pulse cathodic protection in artificial sea water. *Anti-Corros. Methods Mater.* **2007**, *54*, 74–81.
16. Millero, F.J. *Chemical Oceanography*; Taylor & Francis/CRC: Miami, FL, USA, 2006.
17. Yang, Y.; Scantlebury, J.D.; Koroleva, E.V. Under protection of mild steel in seawater and the role of the calcareous film. In Proceedings of the NACE Corrosion Conference, Atlanta, GA, USA, 22–26 March 2009.
18. Pourbaix, M.; Franklin, J.A. *Atlas of Electrochemical Equilibria in Aqueous Solutions*; NACE: Houston, TX, USA, 1966.
19. Evans, U.R. *The Corrosion and Oxidation of Metals*; Edward Arnold & Co.: London, UK, 1960.
20. Ashworth, V.; Booker, C.J.L. *Cathodic Protection, Theory and Practice*; Ellis Horwood: Chichester, UK, 1986.
21. Tseung, S.; Tseung, A.C.C.; Mackay, A.L. The formation of calcareous deposits during the corrosion of mild steel in sea water. *Corros. Sci.* **1986**, *26*, 669–680.
22. Lurie, Y. *Handbook of Analytical Chemistry*; Chimia: Moscow, Russia, 1979.
23. Engell, H.J.; Forchhammer, P. The change of pH under a paint film due to cathodic protection. *Corros. Sci.* **1965**, *5*, 479–484.
24. Packter, A.; Derby, A. Co-precipitation of magnesium iron III hydroxide powders from aqueous solutions. *Cryst. Res. Technol.* **1986**, *21*, 1391–1400.
25. Yang, Y. Calcium and Magnesium Containing Coating Anti-Corrosion Films on Mild Steel. Ph.D. Thesis, University of Manchester, Manchester, UK, 2010.
26. Recommended Practice DHV-RP-B401. Available online: https://exchange.dnv.com/servicedocuments/currentVersion/dnv?DNV-RP-B401 (accessed on 7 December 2014).
27. Refait, Ph.; Abdelmoula, M.; Genin, J.M.R. Mechanisms of formation and structure of green rust one in aqueous corrosion of iron in the presence of chloride ions. *Corros. Sci.* **1998**, *40*, 1547–1560.
28. Heldtberg, M.; MacLeod, I.D.; Richards, V.L. Corrosion and cathodic protection of iron in seawater: A case study of the James Matthews (1841). In Proceedings of the Metal 2004, Acton, Canberra, Australia, 4–8 October 2004.
29. Kolthoff, I.M.; Sandell, E.B.; Machan, E.J.; Bruckenstein, S. *Quantitative Chemical Analysis*; Macmillan: London, UK, 1969.

30. Gordon, L.; Salutsky, M.L.; Willard, H.H. *Precipitation from Homogeneous Solution*; Wiley: New York, NY, USA, 1959.
31. Bologo, V.; Maree, J.P.; Zvinowanda, C.M. Treatment of acid mine drainage using magnesium hydroxide. In Proceedings of the International Mine Water Conference, Pretoria, South Africa, 19–23 October 2009.
32. Chung, S.C.; Cheng, J.R.; Chiou, S.D.; Shih, H.C. EIS behavior of anodized zinc in chloride environments. *Corros. Sci.* **2000**, *42*, 1249–1268.
33. Dobos, D. *Electrochemical Data*; Akademia Kiado: Budapest, Hungary, 1980.